AIAA JOURNAL
Vol. 41, No. 2, February 2003

Split-Domain Harmonic Balance Solutions to Burger's Equation for Large-Amplitude Disturbances

Raymond C. Maple* and Paul I. King†
U.S. Air Force Institute of Technology, Wright–Patterson Air Force Base, Ohio 45433-7765
J. Mitch Wolff‡
Wright State University, Dayton, Ohio 45435
and
Paul D. Orkwis§
University of Cincinnati, Cincinnati, Ohio 45221-0070

A new split-domain harmonic balance approach is presented. The split-domain approach combines the conventional multidomain harmonic balance approach with a split-operator technique in a unique way to solve periodic unsteady flow problems efficiently. The new technique is applied to Burger's equation to obtain solutions for two large-amplitude periodic boundary conditions—a single-frequency sine wave and a simulated wake function. Solutions containing strong moving discontinuities are obtained with Fourier series containing up to 48 frequencies for various grid densities. The split-domain harmonic balance solutions are compared with conventional time-accurate solutions. The differences between the two are found to be asymptotic with respect to the number of Fourier frequencies included. In addition, the harmonic balance approach was found to be sensitive to grid density.

Nomenclature

a = Fourier cosine coefficient
$\tilde{a}$ = amplitude of unsteady input disturbance
b = Fourier sine coefficient
$\tilde{\mathcal{F}}$ = discrete Fourier transform operator
$\hat{\boldsymbol{F}}$ = harmonic balance flux term vector
f = frequency of unsteady input disturbance (1/s)
$\hat{\boldsymbol{S}}$ = harmonic balance source term vector
$\boldsymbol{U}$ = vector of time-sampled dependent variables
$\hat{\boldsymbol{U}}$ = vector of Fourier coefficients
u = scalar dependent variable in Burger's equation
γ = component of frequency domain flux vector
$\Delta\tau$ = pseudotime numerical integration step size
ω = frequency of unsteady input disturbance (rad/s)

Subscripts

i = grid point
n = Fourier frequency number
t = differentiation with respect to time
x = differentiation with respect to space
τ = differentiation with respect to pseudotime

Superscripts

n = time level
T = vector transpose
-1 = operator inverse

Received 21 December 2001; revision received 5 September 2002; accepted for publication 5 September 2002.

*Assistant Professor, Department of Aeronautics and Astronautics, AFIT/ENY, 2950 P. Street, Bldg. 640. Member AIAA.
†Associate Professor, Department of Aeronautics and Astronautics, AFIT/ENY, 2950 P. Street, Bldg. 640. Senior Member AIAA.
‡Associate Professor, Department of Mechanical and Materials Engineering. Associate Fellow AIAA.
§Associate Professor, Department of Aerospace Engineering and Engineering Mechanics, Mail Location 70. Associate Fellow AIAA.

Introduction

UNSTEADY time-periodic flowfields are found in such applications as blade-vane interactions in turbomachinery and aeroelastic limit-cycle oscillations in internal and external flows. Calculations of these flows have typically fallen into one of two categories: time-accurate solutions and linearized solutions. Time-accurate solutions capture nonlinear effects with no restrictions on unsteadiness, but require considerable computation time. Linearized solutions, which are solved using steady-state techniques, are obtained quickly but are limited to small-amplitude unsteadiness and do not capture nonlinear effects.

Recently, methods have been developed to speed up the calculation of problems with significant nonlinear effects. Ning and He, in their unsteady-stress method, included nonlinear effects in a single-frequency, small perturbation solution, with about the same computational effort as the linearized methods.[1] Hall et al. introduced the harmonic balance method to solve a nonlinear system containing a finite number of fully coupled harmonics with no small perturbation assumption, but at the cost of increased problem size.[2] This was accomplished by recasting the dependent variables in the form of a truncated Fourier series in time. As a result, time derivatives were replaced by harmonic frequency source terms, converting the original unsteady problem to a steady-state problem. Convergence acceleration techniques could then be readily employed.

Hall et al.[2] used the harmonic balance method to analyze supersonic flow past a cascade in forced oscillation. In a later work McMullen et al. used the method to model periodic shedding behind a cylinder in crossflow.[3] In both efforts good solutions were obtained with six or fewer frequencies in the approximating Fourier series. A small number of terms was sufficient because the majority of the flowfield contained continuous, relatively small-amplitude unsteadiness. Moving discontinuities either were not present or existed within a very small region of the computational grid. For some problems, however, strong traveling discontinuities can occur, requiring a large number of series terms and a corresponding increase in computational time to achieve an accurate solution.

The purpose of the current study was to examine the behavior of the harmonic balance method in the presence of strong discontinuities moving over large regions of the grid. A useful model for this was the one-dimensional inviscid Burger equation, a simplified form of Euler's equation that yields traveling discontinuities in the flowfield for large-amplitude periodic disturbance boundary conditions. The study included the formulation of the harmonic balance method

for two cases of unsteady boundary conditions, one consisting of a large-amplitude single-frequency sine wave and a second simulating a large-amplitude wake function. Because Burger's equation is hyperbolic and quickly reaches a fully developed solution using time-accurate methods, this model was not suitable for compute-time comparisons between the time-accurate and harmonic balance methods. It did, however, provide a basis for performance comparisons between different harmonic balance implementations.

In recasting Burger's equation into the harmonic balance form, the time-derivative term was replaced by a steady source term. It was found that the presence of this source term reduced the maximum time step allowed for a stable solution below that of the same discretization scheme applied to the standard Burger's equation. To remove this restriction, the authors employed a split-operator technique sometimes used to improve convergence of nonhomogeneous computational fluid dynamics (CFD) problems, such as those involving finite-rate chemistry.[4] The resulting scheme, combined with an efficient two-domain solution approach, is referred to by the authors as the split-domain method. It was found that the split-domain method successfully removed the stability restriction and ran appreciably faster than non-split-domain approaches.

Numerical Method

The one-dimensional inviscid Burger equation is a scalar analog to the one-dimensional Euler equations. It can be formed by considering the Euler momentum equation with constant density and zero pressure gradient:

$$\frac{\partial u}{\partial t} + \frac{1}{2}\frac{\partial (u^2)}{\partial x} = 0 \tag{1}$$

Equation (1) is a common scalar model problem because of its retention of the nonlinear behavior of the Euler equations. Conventional approaches to solving Eq. (1) can be found in most introductory books on CFD, for example, Tannehill et al.[5] and Hoffman and Chiang.[6] Discussions of Fourier series solutions assuming spatial periodicity are also available.[7] A brief development of the harmonic balance form (temporal Fourier series solution) is presented below.

Harmonic Balance Burger's Equation

In this section a brief description of the harmonic balance approach to the one-dimensional inviscid Burger's equation is presented. The dependent variable $u(x, t)$ is approximated by a truncated Fourier series expansion in which the Fourier modes are functions only of time and the Fourier coefficients are functions only of the spatial variable. Though an exponential form can be used, a real Fourier series was employed, the approximation given by

$$u(x, t) \approx a_0 + \sum_{n=1}^{N} [a_n \cos(n\omega t) + b_n \sin(n\omega t)] \tag{2}$$

where $\omega = 2\pi f$ is the fundamental frequency of the expansion in radians per second. Upon substitution into Burger's equation, the time-derivative term becomes

$$u_t \approx \omega \sum_{n=1}^{N} [n b_n \cos(n\omega t) - n a_n \sin(n\omega t)] \tag{3}$$

The flux term is generated by squaring the series and applying trigonometric identities to eliminate products of sines and cosines. Terms in the resulting expression with frequencies higher than in the approximating series are neglected. Upon collection of terms of like frequency and function, the flux term becomes

$$\frac{1}{2}\frac{\partial (u^2)}{\partial x} \approx \frac{1}{2}(\gamma_0)_x + \frac{1}{2}\sum_{n=1}^{N} [(\gamma_{n,a})_x \cos(n\omega t) + (\gamma_{n,b})_x \sin(n\omega t)] \tag{4}$$

where

$$\gamma_0 = a_0^2 + \frac{1}{2}\sum_{n=1}^{N} \left[\left(a_n^2 + b_n^2\right)\right]$$

$$\gamma_{n,a} = 2a_0 a_n + \frac{1}{2}\sum_{l=1}^{N}\sum_{m=1}^{N} [(a_l a_m + b_l b_m)\delta_{|l-m|,n} + (a_l a_m - b_l b_m)\delta_{l+m,n}]$$

$$\gamma_{n,b} = 2a_0 b_n + \sum_{l=1}^{N}\sum_{m=1}^{N} [\mathrm{sign}(m-l) a_l b_m \delta_{|l-m|,n} + a_l b_m \delta_{l+m,n}] \tag{5}$$

In these expressions $\delta_{a,b}$ is the Kronecker delta function, which is equal to 1 if $a = b$ and 0 if $a \neq b$. Substitution of Eqs. (3) and (4) into Burger's equation, Eq. (1), gives

$$(\gamma_0)_x + \sum_{n=1}^{N} [n\omega b_n + (\gamma_{n,a})_x] \cos(n\omega t) + \sum_{n=1}^{N} [-n\omega a_n + (\gamma_{n,b})_x] \sin(n\omega t) = 0 \tag{6}$$

For Eq. (6) to hold for all time, the steady-state expression and the expressions multiplying each sine and cosine must be identically equal to zero. Therefore, the equation can be rewritten as a system of $2N + 1$ coupled steady-state differential equations for $2N + 1$ real Fourier coefficients. Addition of a pseudotime derivative and a rewriting in vector form yields the harmonic balance form of Burger's equation:

$$\hat{\boldsymbol{U}}_\tau + \hat{\boldsymbol{F}}_x + \hat{\boldsymbol{S}} = 0 \tag{7}$$

with

$$\hat{\boldsymbol{U}} = \{a_0, a_1, b_1, \ldots, a_N, b_N\}^T$$

$$\hat{\boldsymbol{S}} = \{0, \omega b_1, -\omega a_1, \ldots, N\omega b_N, -N\omega a_N\}^T$$

$$\hat{\boldsymbol{F}} = \{\gamma_0, \gamma_{1,a}, \gamma_{1,b}, \ldots, \gamma_{N,a}, \gamma_{N,b}\}^T \tag{8}$$

Multidomain Method

The number of operations required to calculate the fluxes using Eq. (4) is of order N^2. Hall et al. pointed out that considerable computational savings is realized by exploiting the relationship between Fourier series coefficients and the frequency response generated by the Fourier transform of the conserved variable u sampled throughout the period of oscillation, at $2N + 1$ evenly spaced moments in time.[2] Defining $\boldsymbol{U}$ as a vector of dependent variable values, $u(x, t)$, sampled at times $t = (0, \Delta t, 2\Delta t, \ldots, 2N\Delta t)$, where $\Delta t = 2\pi/\omega(2N + 1)$, and a Fourier transform operator $\tilde{\mathcal{F}}$ such that $\hat{\boldsymbol{U}} = \tilde{\mathcal{F}}\boldsymbol{U}$, an alternate expression for the flux term is given by

$$\hat{\boldsymbol{F}} \approx \tfrac{1}{2}\tilde{\mathcal{F}}[(\tilde{\mathcal{F}}^{-1}\hat{\boldsymbol{U}})^2] \tag{9}$$

When computed with a modern fast Fourier transform algorithm, the cost of the multidomain calculation (transforming to and from the time domain) lies between order $N \log_2(N)$ and N^2 depending on the value of N. Because the number of samples, $2N + 1$, is always odd, the ideal computational complexity of $N \log_2(N)$ is never achieved. However, for carefully chosen N the total cost of the multidomain flux calculation is close to $N \log_2(N)$, which for larger N is much less than N^2.

Both single-domain [Eq. (4)] and multidomain [Eq. (9)] formulations were investigated, with the multidomain formulation running up to seven times faster than the single-domain formulation for $N = 47$.

Split-Operator Method

Equation (7) was originally implemented with MacCormack's scheme, modified as necessary to include the source terms[8]

$$\hat{\boldsymbol{U}}_i^* = \hat{\boldsymbol{U}}_i^n - \Delta t\left[\left(\frac{\hat{\boldsymbol{F}}_{i+1}^n - \hat{\boldsymbol{F}}_i^n}{2\Delta x}\right) + \hat{\boldsymbol{S}}_i^n\right] \tag{10a}$$

$$\hat{\boldsymbol{U}}_i^{n+1} = \frac{1}{2}\left[\hat{\boldsymbol{U}}_i^n + \hat{\boldsymbol{U}}_i^* - \Delta t\left(\frac{\hat{\boldsymbol{F}}_i^* - \hat{\boldsymbol{F}}_{i-1}^*}{2\Delta x} + \hat{\boldsymbol{S}}_i^*\right)\right] \tag{10b}$$

The inclusion of the harmonic balance source term reduced the stability limit of MacCormack's scheme such that a Courant–Friedrichs–Lewy number (CFL) ≤ 0.6 was required. To improve the stability limit of the system, a second discretization scheme incorporating a split-operator approach was implemented.

The split-operator approach is sometimes used to improve the convergence rates of CFD problems in finite-rate chemistry.[4] The approach is implemented by dividing the inhomogeneous problem into a homogeneous partial differential equation (PDE) and a homogeneous ordinary differential equation (ODE). These two equations are solved alternately using appropriate, possibly different, techniques until the steady-state solution is reached. The split harmonic balance form of Burger's equation is given by

$$\hat{\boldsymbol{U}}_\tau + \hat{\boldsymbol{F}}_x = 0 \tag{11a}$$

$$\hat{\boldsymbol{U}}_\tau = -\hat{\boldsymbol{S}} \tag{11b}$$

For this effort the homogeneous PDE, Eq. (11a), was solved with a standard, explicit MacCormack scheme. The homogeneous ODE, Eq. (11b), was solved using a three-stage Runge–Kutta integration. With this approach the time-step restriction observed in the original implementation was removed.

Split-Domain Scheme

When the multidomain and split-operator techniques were implemented as discussed in the preceding sections, both the PDE and ODE were updated in the frequency domain, and two Fourier transform pairs were required per grid point per iteration, one each for Eqs. (10a) and (10b). With a new approach, referred to as the split-domain scheme, the number of transform pairs was reduced to one per grid point per iteration. Through modification of the multiple-domain approach, the update of the PDE was completed in the time domain and the resulting conserved variables transformed back to the frequency domain.

Defining $\mathcal{M}$ as the update operator for the MacCormack integration and $\mathcal{S}$ as the update operator for the RK integration, one iteration of the split-domain solution process can be represented as a series of operators applied from right to left, each acting on the result of the preceding operation:

$$\hat{\boldsymbol{U}}_i^{n+1} = \mathcal{S}_{\Delta\tau/2}\left[\tilde{\mathcal{F}}\left[\mathcal{M}_{\Delta\tau}\left[\tilde{\mathcal{F}}^{-1}\left[\left[\mathcal{S}_{\Delta\tau/2}\right]\hat{\boldsymbol{U}}_i^n\right]\right]\right]\right] \tag{12}$$

Artificial Dissipation

In all schemes artificial dissipation was required to prevent oscillations near discontinuities in the solution. This was added via a global second-derivative smoothing operation explicitly applied to the Fourier coefficients at the end of each iteration, according to

$$\hat{\boldsymbol{U}}_{i,\text{new}} = \hat{\boldsymbol{U}}_i + \alpha\frac{\hat{\boldsymbol{U}}_{i-1} - 2\hat{\boldsymbol{U}}_i + \hat{\boldsymbol{U}}_{i+1}}{\Delta x^2} \tag{13}$$

The dissipation parameter α was a small constant, of order $1.0E-6$, that controlled the amount of applied damping.

Local Time Stepping

To accelerate convergence to steady state, local time stepping was employed. Using the definition of the CFL limit for Burger's equation, the maximum time step at each point was determined according to

$$\Delta\tau_i = \text{CFL}\frac{\Delta x}{\max(\boldsymbol{U}_i)} \tag{14}$$

where CFL was a user-specified value less than 1.0 and $\max(\boldsymbol{U}_i)$ was the maximum element in the vector of time-sampled dependent variables at grid point i.

Boundary Conditions

Two periodic inflow boundary conditions were modeled. The first, shown in Fig. 1, consisted of a sine wave oscillating about $u = 1$. The second, shown in Fig. 2, was a simulated wake function consisting of a uniform value ($u = 1$) interrupted over one-quarter of its period by a sine-squared waveform. Mathematically, these input conditions were given by

$$u(0, t) = 1.0 + \tilde{a}\sin(2\pi f t) \tag{15a}$$

$$u(0, t) = \begin{cases} 1.0 & 0 \leq t < 3/4f \\ 1.0 + \tilde{a}\sin^2(4\pi f) & 3/4f \leq t \leq 1/f \end{cases} \tag{15b}$$

where $\tilde{a}$ was the amplitude and f the reduced temporal frequency of the oscillations.

For $u > 0.0$ the input boundary conditions for the harmonic balance Burger's equation are constants equal to the Fourier series coefficients of the input waveforms. These were calculated using

$$a_0 = 1.0, \qquad a_n = 0.0, \qquad 1 \leq n \leq N$$

$$b_n = \begin{cases} \tilde{a} & n = 1 \\ 0.0 & 1 < n \leq N \end{cases} \tag{16a}$$

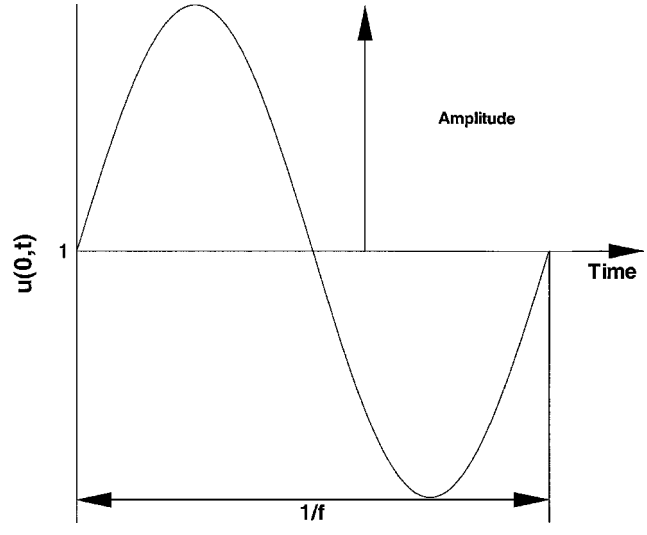

Fig. 1 Sine inflow boundary condition.

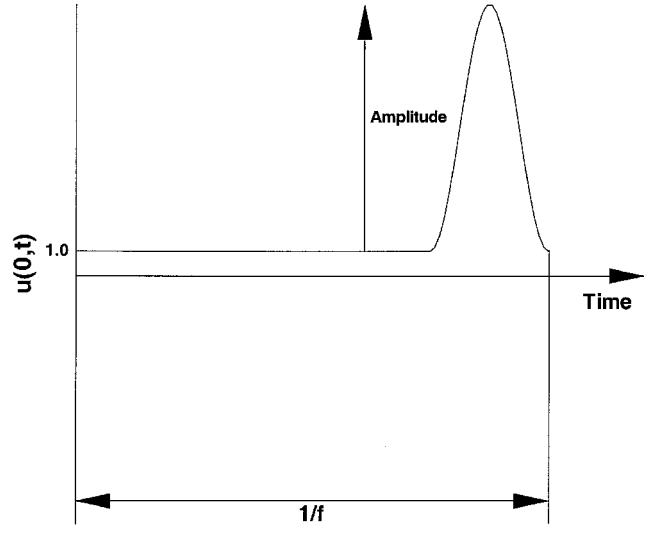

Fig. 2 Wake function inflow boundary condition.

$$a_0 = 1 + 0.125\tilde{a}$$

$$a_n = \begin{cases} \dfrac{8\tilde{a}}{n(n^2-16)\pi}\left[\sin\left(\dfrac{n\pi}{2}\right)\right], & 1 \le n \le N,\ n \ne 4 \\ -0.125\tilde{a} & n = 4 \end{cases}$$

$$b_n = \begin{cases} \dfrac{8\tilde{a}}{n(n^2-16)\pi}\left[\cos(n\pi) - \cos\left(\dfrac{n\pi}{2}\right)\right], & 1 \le n \le N,\ n \ne 4 \\ 0.0 & n = 4 \end{cases} \tag{16b}$$

for the sine and wake function inputs, respectively.

Because Burger's equation is hyperbolic and the test problems contained only positive values of the dependent variable in the time domain, all information traveled from inside to outside the outflow boundary. Simple extrapolation of the dependent variables was therefore used for the outflow boundary conditions.

Results

Solutions were obtained for both input waveforms with varying amplitudes ($\tilde{a} = 0.1,\ 0.3,\ 0.5$) and temporal, reduced frequencies ($f = 0.75,\ 1.5,\ 3.0$). Solutions are shown for each input variation in Figs. 3 and 4. These figures compare the solution at $t = 0$ relative to the input period with an equivalent fully developed time-accurate calculation. The harmonic balance solutions were based on a 48-frequency approximating series computed on a 501 point grid. The time-accurate solutions were obtained on the same grid using a validated MacCormack scheme solver with the same artificial dissipation used for the harmonic balance equation, Eq. (13).

As Figs. 3 and 4 show, the input boundary conditions resulted in solutions ranging from smooth traveling waves to strong moving discontinuities. In all but two cases, the 48 frequency harmonic balance solutions were comparable to the time-accurate solutions. The two exceptions were the sine input cases with amplitudes $\tilde{a} = 0.5$ and 0.3 at the lowest disturbance frequency. These cases contain significant high-frequency oscillations in their solutions. It will be shown in the next section that these cases require additional terms in the approximating series.

Series Length and Accuracy

To determine the effect of series length on the accuracy of the harmonic balance method, solutions were generated for each input condition with series lengths ranging from 2 to 48 frequencies. A quantitative measure of the difference between each of these solutions

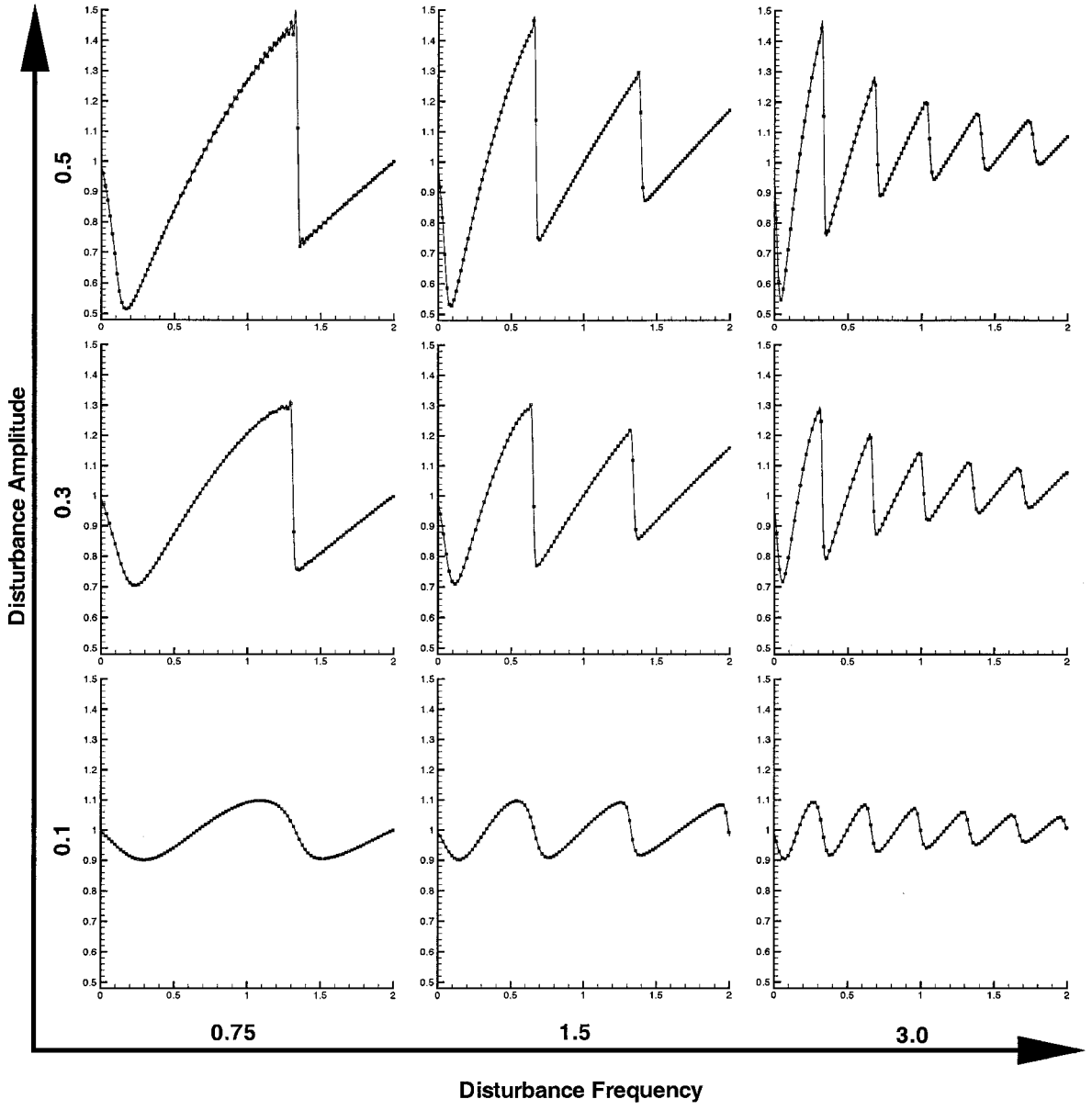

Fig. 3 Comparison of time-accurate (——) and 48-frequency harmonic balance (symbols) solutions for the sine input for $t = 0$. Inset plots show dependent variable u magnitude vs nondimensional distance.

and an equivalent time-accurate solution was obtained by calculating the difference rms for 10 equally spaced temporal samples spanning one period of the disturbance. These 10 rms differences were averaged to obtain a solution difference. The results are plotted in Figs. 5 and 6.

The results show that the differences between the harmonic balance and time-accurate solutions did not go to zero but were asymptotic with respect to approximating series length. In each case where a good solution was obtained, there was a series length corresponding to some Fourier frequency beyond which no improvement occurred. This frequency is hereafter referred to as the asymptotic frequency, and the associated solution is called the asymptotic solution. Solutions based on fewer frequencies are called subasymptotic, whereas those with more frequencies are called superasymptotic. It is clear from Fig. 5 that the two cases with oscillatory solutions are subasymptotic and thus required additional frequencies to minimize error.

The fact that the differences between the harmonic balance and time-accurate solutions were asymptotic with respect to series length does not mean that the harmonic balance solutions did not continue to converge. The truncation error in the harmonic balance solution simply became insignificant compared to differences caused by other factors such as a slight difference in shock location.

Both disturbance amplitude and disturbance frequency influenced the asymptotic frequency. As amplitude increased, the asymptotic frequency increased. This was attributed to the presence of stronger discontinuities in the larger amplitude solutions. In contrast, as the disturbance frequency increased the asymptotic frequency usually decreased. This behavior is explained qualitatively.

If the shape and period of the time response of Burger's equation at every point in the grid is fixed, the response then has a fixed frequency content with significant energy up to some frequency $\omega_{\max}$. In the harmonic balance solution $\omega_{\max}$ is expressed as some multiple of the fundamental frequency, say $n_{\max}\omega$. Then $n_{\max} = \omega_{\max}/\omega$ is inversely proportional to ω, increasing as ω decreases.

True inverse proportionality was observed in some test cases (e.g., the sine input with frequency change from $f = 1.5$ to 3.0, all amplitudes), but for the majority of the cases the asymptotic frequency was less than that predicted by the simple model. This is consistent with the fact that a discontinuity in the time response is generally sharper for higher disturbance frequencies, and thus $\omega_{\max}$ is not constant.

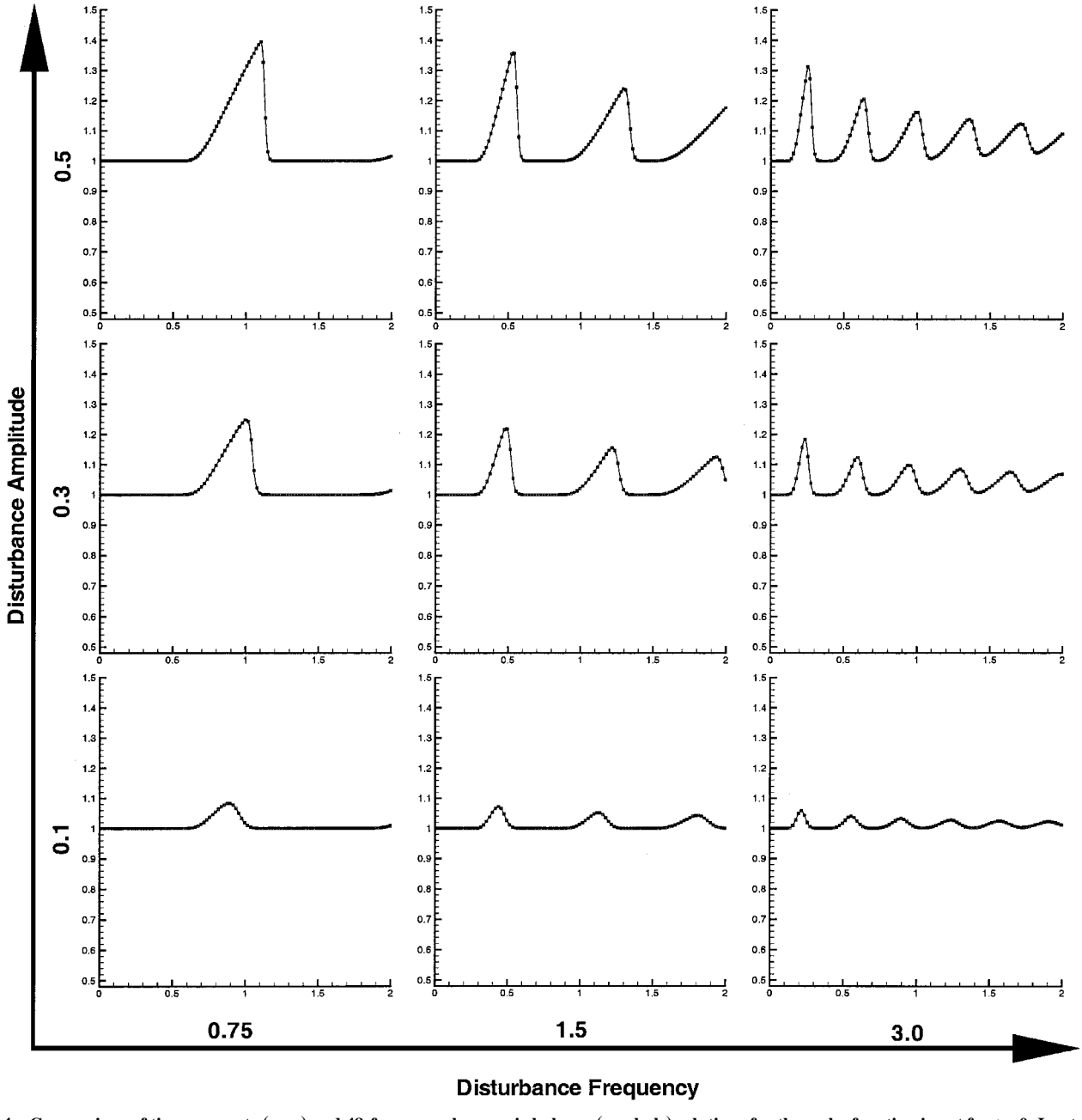

Fig. 4 Comparison of time-accurate (——) and 48-frequency harmonic balance (symbols) solutions for the wake function input for $t = 0$. Inset plots show dependent variable u magnitude vs nondimensional distance.

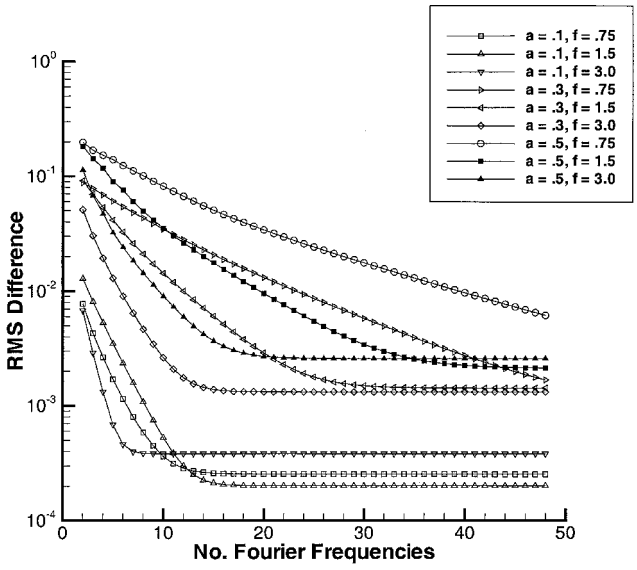

Fig. 5 RMS difference between time-accurate and harmonic balance solutions for different series lengths: sine inflow boundary condition.

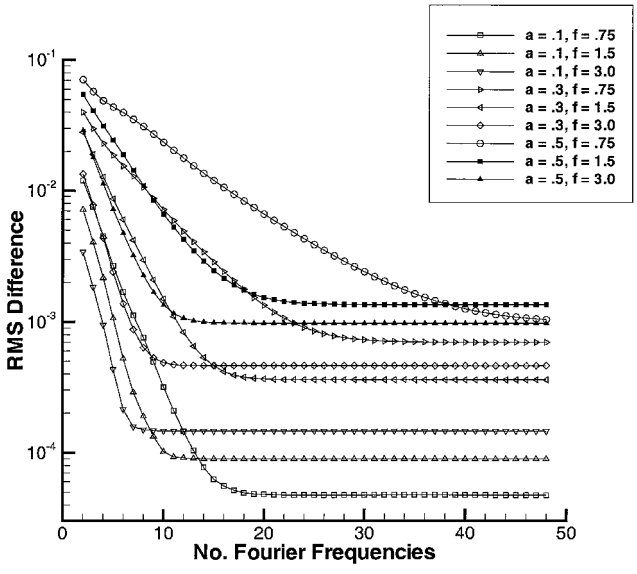

Fig. 6 RMS difference between time-accurate and harmonic balance solutions for different series lengths: wake function inflow boundary condition.

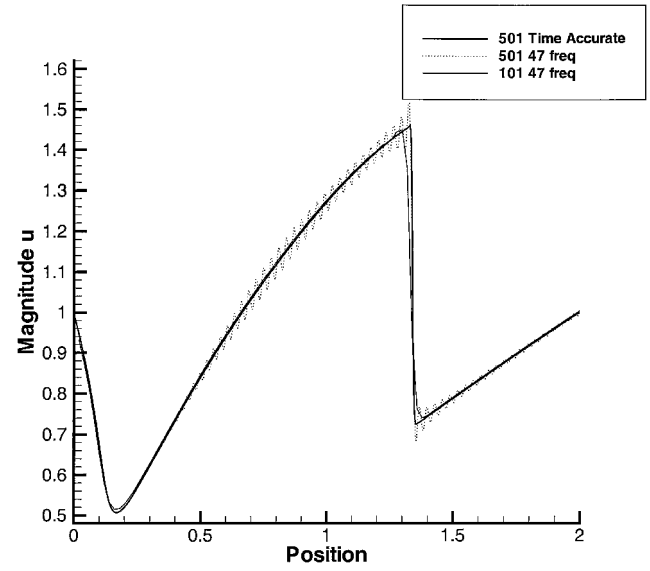

Fig. 7 Reduction of high-frequency oscillations in harmonic balance solution on coarse grid.

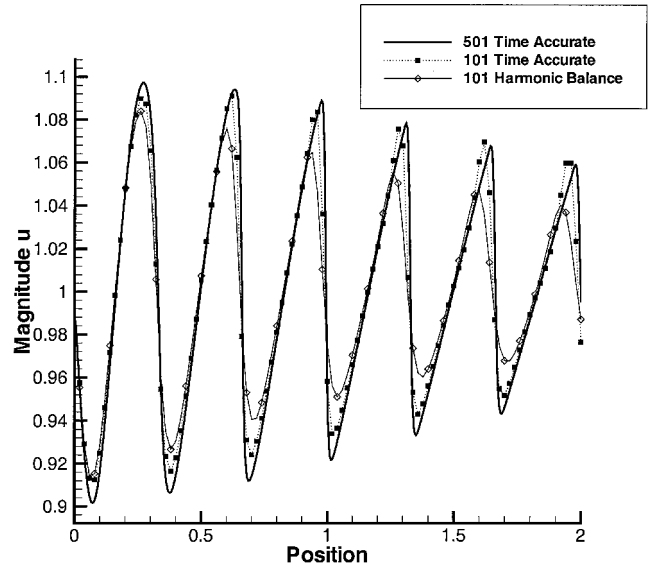

Fig. 8 Damping of harmonic balance solution on coarse grid.

Series Length and Stability

For superasymptotic solutions increased series length sometimes had a detrimental effect on numerical stability. All subasymptotic and asymptotic solutions, however, were successfully converged to a residual (measured as the rms of the change in $\hat{U}$ over the grid) of $5.0E-8$ with a CFL of 0.95, independent of the number of frequencies used.

The need for a reduced CFL was not consistently related to the number of superasymptotic frequencies included in the solution. Only test cases with a disturbance frequency of 3.0 required a reduced CFL to obtain 48-frequency solutions. In these cases reductions of 40–60% in CFL were required. All other test cases converged with an unreduced CFL, despite the fact that some of those cases had smaller asymptotic frequencies than some of the $f=$ 3.0 cases.

Effect of Grid Density

All of the harmonic balance solutions became dissipative to some degree as the computational grid was coarsened. The impact on solution quality depended on the nature of the flowfield. For solutions with strong discontinuities, the effect was relatively minor, and sometimes beneficial, whereas for smooth, small-amplitude solutions the effect introduced severe damping.

One example of a beneficial dissipative effect is shown in Fig. 7. This figure shows that although the coarse grid solution experiences some smearing of the shock there is almost complete elimination of the nonphysical oscillations present in the 47-frequency fine-grid solution. Eliminating these oscillations on a fine grid would require the use of a much longer approximating Fourier series.

An example of unfavorable effect of a coarse grid is illustrated in Fig. 8. This figure compares the 501-point time-accurate solution, the 101-point time-accurate solution, and the 101-point harmonic balance solution. The coarse-grid, time-accurate solution shows some degradation, primarily in the form of a phase lag in the peaks of the solution. In contrast, the coarse-grid damping effect caused considerable degradation in the harmonic balance solution. The harmonic balance method was more sensitive to grid density than the time-accurate method.

The effect of grid density in both cases was traced to the Fourier coefficients corresponding to the higher computed frequencies. Figure 9a shows the variation in magnitude of one high-frequency ($n=47$) coefficient for the $\tilde{a}=0.5$, $f=0.75$ sine input on the 501-point grid. The computed coefficient shows rapid oscillation in the spatial dimension. Figure 9b shows the same coefficient calculated on the 101-point grid. In this case the coarse grid did not contain sufficient spatial resolution to capture the oscillations

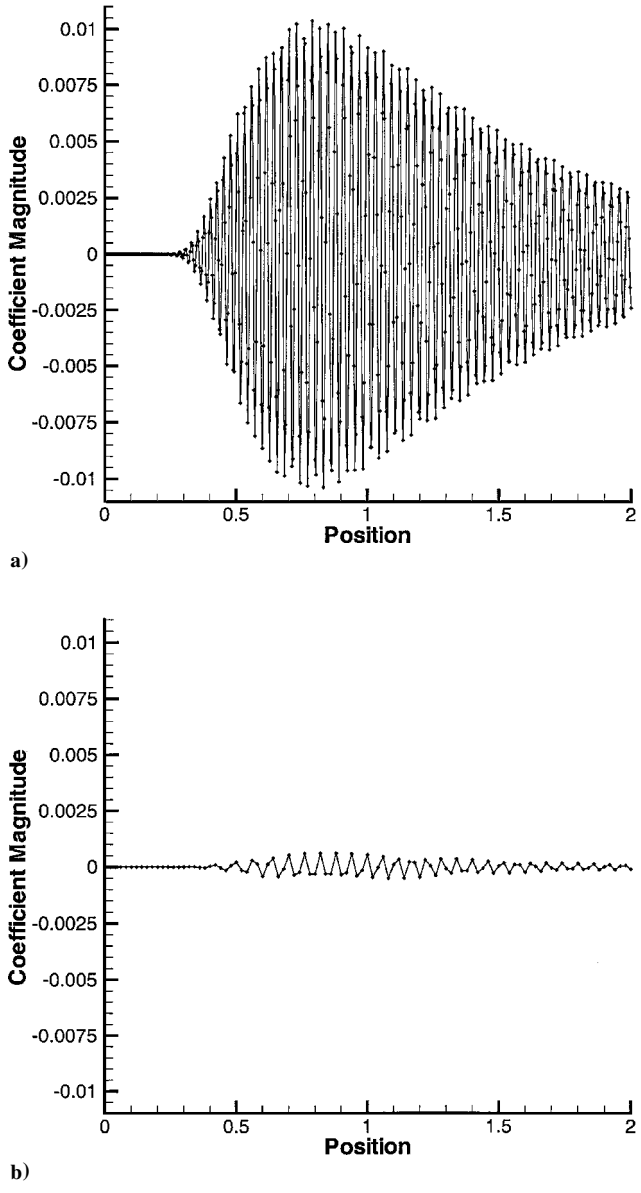

Fig. 9 Information loss in high-frequency coefficient on coarse grid: a) fine (501-point) and b) coarse (101-point) grids.

in magnitude, and the magnitude of the coefficient was underpredicted. The impact of poorly resolved high-frequency coefficients depended on the relative importance of those frequencies in the harmonic balance solution. In the case shown in Fig. 7, most of the energy in the solution was contained in relatively low frequencies, and coarse-grid damping of the highest frequencies resulted in beneficial smoothing. For the case shown in Fig. 8, however, the damped frequencies comprised a significant part of the solution, and the overall accuracy was degraded.

The results show that although grid density is important for harmonic balance solutions grid density is even more important for smooth solutions that require fewer terms in the approximating series. Problems that require many terms might require less grid resolution, partially offsetting the cost of the additional terms.

Performance

For longer series lengths the split-domain solver took significantly less time to calculate a solution. For a typical 47-frequency solution the split-domain solver ran approximately three times faster than the nonsplit multidomain solver and seven times faster than the single-domain solver. Factors contributing to the reduced run time were the larger time step allowed by the higher CFL and the calculation of fluxes in the time domain with only a single Fourier transform pair. Performance improvement was highly dependent on series length, however. For a series length of 48, the split-domain solver ran approximately 4.3 times faster than the nonsplit multidomain solver, but only 1.8 times faster than the single-domain solver.

Conclusions

Large-amplitude, time-periodic solutions to Burger's equation were computed with a harmonic balance method employing a new split-domain technique. The new technique combined the conventional multidomain harmonic balance approach with a split-operator method. The split-domain technique allowed efficient calculation of the fluxes (multidomain approach), eliminated an observed time-step restriction caused by the inhomogeneity in the harmonic balance form of Burger's equation (split-operator technique), and reduced the number of transitions between domains required for each iteration (application of split operators in different domains). Solutions for boundary conditions containing moving waves ranging from smooth disturbances to strong discontinuities were successfully modeled with the split-domain harmonic balance method. Comparison with conventional time-accurate calculations showed that the error in the harmonic balance solutions was asymptotic with respect to the number of frequencies included in the approximating solution. Several factors were found to influence the asymptotic frequency, including disturbance frequency, the strength of the moving wave, and the computational grid density.

Although these results were obtained for a low-order model (Burger's equation), the split-domain technique can be applied to higher-order models.

Acknowledgments

This project was funded by the State of Ohio under the auspices of the Dayton Area Graduate Studies Institute, Frank Moore, Director, Project PR-AFIT-99-07. The views expressed in this paper are those of the authors and do not reflect the official policy or position of the U.S. Air Force, the Department of Defense, or the U.S. Government.

References

[1]Ning, W., and He, L., "Computation of Unsteady Flows Around Oscillating Blades Using Linear and Nonlinear Harmonic Euler Methods," *Journal of Turbomachinery*, Vol. 120, No. 3, 1998, pp. 508–514.

[2]Hall, K., Thomas, J., and Clark, W., "Computation of Unsteady Nonlinear Flows in Cascades Using a Harmonic Balance Technique," 9th International Symposium on Unsteady Aerodynamics, Aeroacoustics, and Aeroelasticity of Turbomachines, Tech. Rept., Sept. 2000.

[3]McMullen, M., Jameson, A., and Alonso, J. J., "Acceleration of Convergence to a Periodic Steady State in Turbomachinery Flows," AIAA Paper 2001-0152, Jan. 2001.

[4]Schwer, D. A., and Green, W. H., Jr., "Split-Operator Methods for Computing Steady-State Reacting Flow Fields," AIAA Paper 2001-2635, June 2001.

[5]Tannehill, J. C., Anderson, D. A., and Pletcher, R. H., *Computational Fluid Mechanics and Heat Transfer*, 2nd ed., Taylor and Francis, Philadelphia, 1997, pp. 176–217.

[6]Hoffman, K. A., and Chiang, S. T., *Computational Fluid Dynamics*, 4th ed., Vol. I, Engineering Education System, Wichita, KS, 2000, pp. 206–227.

[7]Duran, D. R., *Numerical Methods for Wave Equations in Geophysical Fluid Dynamics*, Springer-Verlag, New York, 1999, pp. 173–240.

[8]LeVeque, R. J., and Yee, H. C., "A Study of Numerical Methods for Hyperbolic Conservation Laws with Stiff Source Terms," *Journal of Computational Physics*, Vol. 86, No. 1, 1990, pp. 187–210.

P. Givi
Associate Editor